

Proceedings of the Institution of Mechanical Engineers, Part I: Journal of Systems and Control Engineering

<http://pii.sagepub.com/>

Output feedback image-based visual servoing control of an underactuated unmanned aerial vehicle

Hamed Jabbari Asl, Giuseppe Oriolo and Hossein Bolandi

Proceedings of the Institution of Mechanical Engineers, Part I: Journal of Systems and Control Engineering 2014 228: 435

originally published online 8 May 2014

DOI: 10.1177/0959651814530698

The online version of this article can be found at:

<http://pii.sagepub.com/content/228/7/435>

Published by:



<http://www.sagepublications.com>

On behalf of:



[Institution of Mechanical Engineers](http://www.imechE.org)

Additional services and information for *Proceedings of the Institution of Mechanical Engineers, Part I: Journal of Systems and Control Engineering* can be found at:

Email Alerts: <http://pii.sagepub.com/cgi/alerts>

Subscriptions: <http://pii.sagepub.com/subscriptions>

Reprints: <http://www.sagepub.com/journalsReprints.nav>

Permissions: <http://www.sagepub.com/journalsPermissions.nav>

Citations: <http://pii.sagepub.com/content/228/7/435.refs.html>

[OnlineFirst Version of Record - May 8, 2014](#)

[What is This?](#)

Output feedback image-based visual servoing control of an underactuated unmanned aerial vehicle

Proc IMechE Part I:
J Systems and Control Engineering
2014, Vol. 228(7) 435–448
© IMechE 2014
Reprints and permissions:
sagepub.co.uk/journalsPermissions.nav
DOI: 10.1177/0959651814530698
pii.sagepub.com


Hamed Jabbari Asl¹, Giuseppe Oriolo² and Hossein Bolandi¹

Abstract

In this article, image-based visual servoing control of an underactuated unmanned aerial vehicle is considered for the three-dimensional translational motion. Taking into account the low quality of accelerometers' data, the main objective of this article is to only use information of rate gyroscopes and a camera, as the sensor suite, in order to design an image-based visual servoing controller. Kinematics and dynamics of the unmanned aerial vehicle are expressed in terms of visual information, which make it possible to design dynamic image-based visual servoing controllers without using linear velocity information obtained from accelerometers. Image features are selected through perspective image moments of a flat target plane in which no geometric information is required, and therefore, the approach can be applied in unknown environments. Two output feedback controllers that deal with uncertainties in dynamics of the system related to the motion of the target and also unknown depth information of the image are proposed using a linear observer. Stability analysis guarantees that the errors of the system remain uniformly ultimately bounded during a tracking mission and converge to 0 when the target is stationary. Simulation results are presented to validate the designed controllers.

Keywords

Visual servoing, unmanned aerial vehicle, observer, image moments

Date received: 26 April 2013; accepted: 30 January 2014

Introduction

Increasing applications of unmanned aerial vehicles (UAVs) have motivated researchers to improve their capabilities through developing new control strategies and integrating suitable sensors. Although there are robust sensor systems in the market that provide significant information for the vehicle stabilization, cost and weight are the two important factors that limit using those sensors in the small-scale UAVs. The sensor system for an UAV generally includes an inertial measurement unit (IMU) and a Global Positioning System (GPS). Commonly used IMU systems provide reliable information for angular velocity and attitude of these vehicles, but in contrast translational position and linear velocity information cannot be effectively estimated by these systems. On the other hand, GPSs do not function properly when the application of interest involves indoor environment.

Vision sensor is a reliable and low-cost system, which can be fused with the IMU data to provide useful translational velocity information and also can be effectively used in localization of a vehicle with respect

to its environment. In the last decade, vision system has received a great attention for aerial vehicles and many applications have been reported for these robots including estimation of ego-motion,¹ pose estimation,² simultaneous localization and mapping (SLAM),³ automatic landing,⁴ positioning,⁵ obstacle avoidance⁶ and so on. In some of these applications, vision information is directly used in the design of controller.

Attention to control the flying robots using vision-based methods rose from the late 1990s. Vision-based control of robots mainly includes two major approaches. One approach is position-based visual servoing (PBVS) where control is on Cartesian space,

¹Department of Electrical Engineering, Iran University of Science and Technology, Tehran, Iran

²Dipartimento di Ingegneria Informatica, Automatica e Gestionale, Sapienza University of Rome, Rome, Italy

Corresponding author:

Hamed Jabbari Asl, Department of Electrical Engineering, Iran University of Science and Technology, Narmak, Tehran 1684613114, Iran.
Email: hjabbari@just.ac.ir

based on three-dimensional (3D) information of workspace reconstructed from two-dimensional (2D) image data. Implementation of this approach on the aerial vehicles has been reported in some works including Altug et al.,^{7,8} and Garca Carrillo et al.⁹ Pose estimation is the major challenge in PBVS approach. Most of the developed algorithms for this purpose need prior information from geometric model of the observed target. Improving accuracy of the estimation approaches increases the computations and requires noiseless image data; besides, most of the proposed approaches are sensitive to initial conditions.¹⁰ The other approach is image-based visual servoing (IBVS) in which control is based on dynamics of image features in the image plane. IBVS does not need 3D information reconstruction and so is simpler in computations with respect to PBVS. This approach is also robust with respect to camera calibration errors. However, IBVS method still needs depth information of the observed image features.

Implementation of IBVS approach for dynamic underactuated UAV systems requires more challenge in designing the controller. Passivity properties of spherical image moments are used in Hamel and Mahony^{5,11} and Guenard et al.¹² to design full dynamic IBVS controllers for cascade dynamics of a quadrotor helicopter. However, the selected image features do not provide satisfactory behavior of the robot in vertical axis, which is addressed and slightly improved by rescaled spherical image moments in Bourquardez et al.¹³ To overcome this conditioning problem, we have proposed a method in Jabbari Asl et al.,¹⁴ which utilizes perspective image moments and the control is based on their dynamics in an oriented image plane.

In all the mentioned works for IBVS, the design is based on this assumption that correct measurement of translational velocity of the vehicle is available. Considering the stated problem to obtain this information, optic flow of image features is used in Mahony et al.¹⁵ as a cue of translational velocity and dynamics of the system are expressed based on dynamics of spherical optic flow. However, the designed full dynamic IBVS controller has the conditioning problem mentioned above. An observer-based method has been presented in Le Bras et al.¹⁶ where two nonlinear observers are used to estimate translational velocity and attitude of the system. This approach provides only a basin of attraction for the system and needs to estimate attitude of the vehicle from image information, which requires prior geometrical information from model of the observed target and visual tracking of image features. Furthermore, these works are only developed for the case that the target is stationary.

In this article, we present two observer-based dynamic IBVS controllers for controlling the 3D translational motion of a quadrotor helicopter. Our control laws utilize perspective image features reconstructed in a suitably defined virtual image plane. These features are used in the earlier work by Jabbari Asl et al.,¹⁷

which provide efficient trajectories in both image and Cartesian space. Kinematics and dynamics of the system are expressed in terms of the dynamics of the velocity of the image features, which make it possible to design dynamic IBVS controllers without using linear velocity information. The first controller is robust with respect to uncertainties of the system including the unknown motion of the target and the depth information of the image. In the second controller, an adaptive scheme is developed in order to compensate the unknown depth uncertainty if the target is stationary. A linear observer is used in order to estimate the velocity of the image features. Another advantage of our approaches over previous ones is that the yaw angle of the UAV is not required in them to design the visual control laws. Stability analysis shows that the system states are uniformly ultimately bounded (UUB) and the errors converge to a small adjustable compact set during a tracking mission and converge to 0 when the target is stationary.

The rest of the article is organized as follows. Section "Equations of motion of the robot" presents kinematics and dynamics models of the quadrotor helicopter. In section "Image dynamics," image features are introduced and their dynamics in the new image plane are presented. The proposed observer-based IBVS controllers, designed for the translational motion of the robot, are given in section "Observer-based IBVS using image features as outputs." Simulation results are presented in section "Simulation results." Finally, conclusions are given in section "Conclusion."

Equations of motion of the robot

In this section, we describe the kinematics and dynamics models of the quadrotor helicopter (Figure 1). The models are similar to those introduced in the literature, for example, Tayebi and McGillvray.¹⁸ Two coordinate frames are considered for describing the equations of the motion of the quadrotor equipped with a down-looking camera, which define the motion of the camera. They include an inertial frame $\mathcal{I} = \{O_i, X_i, Y_i, Z_i\}$ and a body-fixed frame $\mathcal{B} = \{O_b, X_b, Y_b, Z_b\}$, which is attached to the center of

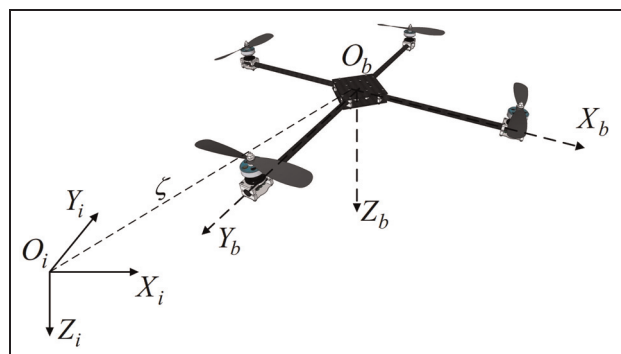


Figure 1. Quadrotor helicopter.

mass of the robot. The center of the frame \mathcal{B} is located in position $\zeta = (x, y, z)$ with respect to the inertial frame and its attitude is given by the orthogonal rotation matrix $\mathbf{R} : \mathcal{B} \rightarrow \mathcal{I}$ depending on the three Euler angles ϕ , θ and ψ denoting the roll, the pitch and the yaw, respectively.

Considering $\mathbf{V} \in \mathbb{R}^3$ and $\mathbf{\Omega} = [\Omega_1 \Omega_2 \Omega_3]^T$ as linear and angular velocities of the robot in the body-fixed frame, respectively, we say that the kinematics of the quadrotor as a 6-degree-of-freedom (DOF) rigid body are as follows

$$\begin{aligned} \dot{\zeta} &= \mathbf{R}\mathbf{V} \\ \dot{\mathbf{R}} &= \mathbf{R}sk(\mathbf{\Omega}) \end{aligned}$$

The notation $sk(\mathbf{\Omega})$ is the skew-symmetric matrix such that for any vector $\mathbf{b} \in \mathbb{R}^3$, $sk(\mathbf{\Omega})\mathbf{b} = \mathbf{\Omega} \times \mathbf{b}$ where \times denotes the vector cross product. The relation between time derivatives of the Euler angles and the angular velocities is given by

$$\begin{bmatrix} \dot{\phi} \\ \dot{\theta} \\ \dot{\psi} \end{bmatrix} = \begin{bmatrix} 1 & \sin \phi \tan \theta & \cos \phi \tan \theta \\ 0 & \cos \phi & -\sin \phi \\ 0 & \sin \phi / \cos \theta & \cos \phi / \cos \theta \end{bmatrix} \begin{bmatrix} \Omega_1 \\ \Omega_2 \\ \Omega_3 \end{bmatrix} \quad (1)$$

The dynamics of a general 6-DOF rigid body, with the mass of m and the constant symmetric inertial matrix $\mathbf{J} \in \mathbb{R}^{3 \times 3}$ around the center of mass, can be expressed in the frame \mathcal{B} using Newton–Euler’s equations as follows

$$\begin{aligned} \dot{\mathbf{V}} &= -\mathbf{\Omega} \times \mathbf{V} + \mathbf{F} \\ \mathbf{J}\dot{\mathbf{\Omega}} &= -\mathbf{\Omega} \times \mathbf{J}\mathbf{\Omega} + \boldsymbol{\tau} \end{aligned} \quad (2)$$

where $\mathbf{F} \in \mathbb{R}^3$ (scaled by m) and $\boldsymbol{\tau} \in \mathbb{R}^3$ are the force and the torque vectors in the frame \mathcal{B} , respectively, which determine specific dynamics of the system. The inertial matrix is diagonal, $\mathbf{J} = \text{diag}(J_{xx}, J_{yy}, J_{zz})$, when O_b is coincident with the body principal axis of inertia. The quadrotor actuators generate a single actuation trust input, U_1 , and full actuation of the torque $\boldsymbol{\tau} = [U_2 \ U_3 \ U_4]^T$; this demonstrates underactuated dynamics of the system. The force input \mathbf{F} in equation (2) is as follows

$$\mathbf{F} = -\frac{1}{m}U_1\mathbf{E}_3 + g\mathbf{R}^T\mathbf{e}_3 \quad (4)$$

where $\mathbf{E}_3 = \mathbf{e}_3 = [0 \ 0 \ 1]^T$ are the unit vectors in the body-fixed frame and the inertial frame, respectively. Note that the term $\mathbf{R}^T\mathbf{e}_3$ and, hence, the translational dynamics do not depend on the yaw angle. Therefore, the yaw dynamics can be controlled independently from the translational dynamics.

For visual servoing of quadrotor, the full dynamics of the system have sometimes been taken into account in designing the controller.^{11,14} However, another approach is the separation of the control problem into inner-loop and outer-loop control. The inner-loop, which uses inputs from rate gyroscopes acquired at high data rate, regulates the torque inputs to track a

desired orientation. This desired orientation is defined by the outer loop through an IBVS scheme. Time-scale separation and high-gain arguments can be used to ensure the stability of the whole system.¹⁹ Here, we will only consider control of the translational dynamics and assume that a suitable high-gain inner-loop controller provides the desired torque for the system’s attitude.

Image dynamics

Commonly used image formations for visual servoing are perspective and spherical projection. It is shown in Bourquardez et al.¹³ that perspective image moments do not guarantee global stability of the system for IBVS control of a quadrotor. On the other hand, although spherical image moments, because of passivity properties of their dynamics, satisfy stability conditions for IBVS, they do not provide suitable behavior in Cartesian coordinates trajectories of the robot. Besides, in order to preserve the passivity properties for the dynamics of the image error, it is necessary to use full rotational information of the camera.^{5,11,12} In order to deal with the mentioned problems, we have proposed a method in Jabbari Asl et al.,¹⁴ which uses appropriately defined perspective image moments that are reprojected on an oriented image plane, called virtual image plane, using only roll and pitch angles of the robot. Properties of the dynamics of the selected image features in the new image plane make it possible to design full dynamic image-based controller for the underactuated UAV while preserving a good behavior of the robot in Cartesian space. In this article, the same imaging method is used for IBVS control of the quadrotor considering the velocity of image features.

In the remainder of this section, we first present the dynamics of a point in the virtual image plane and then define image features that are used in section “Observer-based IBVS using image features as outputs” to design the visual servo controllers.

Projection of image points in a new image plane

Suppose that ${}^{\mathcal{I}}\mathbf{p}(t)$ are the coordinates of a moving point P relative to the inertial frame, \mathcal{I} . Also, consider the frame $\mathcal{C} = \{O_c, X_c, Y_c, Z_c\}$, which is called camera frame and is attached to the center of projection of a moving camera, where its X_c - and Y_c -axes are parallel with the horizontal and vertical axes of the image plane, respectively, and its Z_c -axis is perpendicular to the image plane, passing through the focal center of the lens. The origin of this frame, O_c , is located at a distance λ (the focal length) behind the image plane. Now, we consider a new coordinate frame, $\mathcal{V} = \{O_v, X_v, Y_v, Z_v\}$, and an image plane named virtual frame and virtual image plane, respectively. Position and orientation of the virtual image plane with respect to \mathcal{V} is the same as the image plane with respect

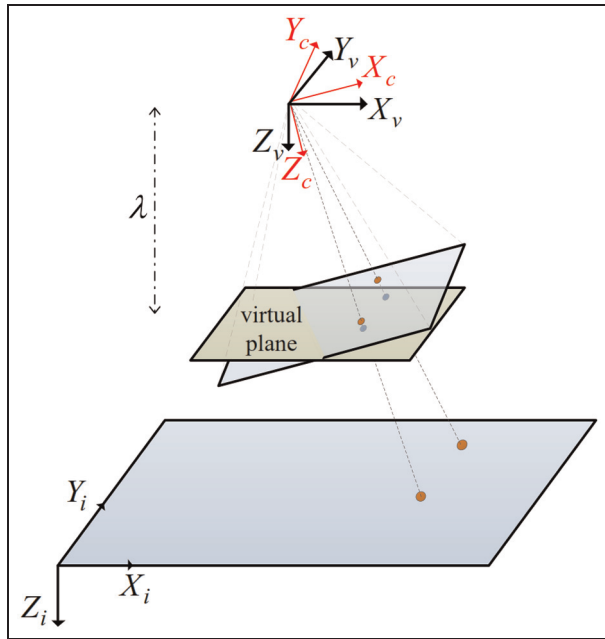


Figure 2. Camera and virtual coordinate frames and image planes.

to \mathcal{C} (Figure 2). The virtual frame moves with the camera frame, but it does not inherit its dynamics around X_c - and Y_c -axes (i.e. the $X_v Y_v$ plane is always parallel to $X_i Y_i$ plane). Thus, coordinates of the point P relative to the virtual frame at time t will be

$${}^v \mathbf{p}(t) = \mathbf{R}_\psi^T(t) [{}^I \mathbf{p} - \mathbf{O}_v(t)]$$

where $\mathbf{R}_\psi(t)$ is the rotation matrix around Z_i at time t . Then, the time derivative of ${}^v \mathbf{p}(t) = [{}^v p_x \quad {}^v p_y \quad {}^v p_z]^T$ will be

$$\begin{aligned} \frac{d}{dt} {}^v \mathbf{p}(t) &= \left(\frac{d}{dt} \mathbf{R}_\psi \right)^T ({}^I \mathbf{p} - \mathbf{O}_v) - \mathbf{R}_\psi^T \dot{\mathbf{O}}_v + \mathbf{R}_\psi^{TT} \dot{\mathbf{p}} \\ &= -sk(\dot{\psi} \mathbf{e}_3) {}^v \mathbf{p} - \mathbf{v} + \Delta_1 \end{aligned} \quad (5)$$

For simplicity, time dependency is not shown for the variables. In equation (5), vector $\mathbf{v}(t) = [{}^v v_x \quad {}^v v_y \quad {}^v v_z]^T$ is the linear velocity of the camera frame expressed in the virtual frame and $\Delta_1(t) = [d_x \quad d_y \quad d_z]^T$ is the velocity of the moving point in the virtual frame.

$\mathbf{R}_{\phi\theta}$, the rotation matrix, respectively, around X_i and Y_i , can be used to reproject the image coordinates (u, n) in the image plane to the virtual image plane as follows

$$\begin{bmatrix} {}^v u \\ {}^v n \\ \lambda \end{bmatrix} = \beta \mathbf{R}_{\phi\theta} \begin{bmatrix} u \\ n \\ \lambda \end{bmatrix}, \beta = \frac{\lambda}{\left([0 \ 0 \ 1] \mathbf{R}_{\phi\theta} \begin{bmatrix} u \\ n \\ \lambda \end{bmatrix} \right)} \quad (6)$$

By using equation (5) and well-known perspective projection equations, which are defined as ${}^v u = \lambda({}^v x)/({}^v z)$ and ${}^v n = \lambda({}^v y)/({}^v z)$, relation of the velocity of the image coordinates of a moving point in

the virtual plane with the velocity of the camera frame in a matrix form will be¹⁴

$$\begin{bmatrix} {}^v \dot{u} \\ {}^v \dot{n} \end{bmatrix} = \begin{bmatrix} -\frac{\lambda}{{}^v z} & 0 & \frac{{}^v u}{{}^v z} \\ 0 & -\frac{\lambda}{{}^v z} & \frac{{}^v n}{{}^v z} \end{bmatrix} \begin{bmatrix} {}^v v_x - d_x \\ {}^v v_y - d_y \\ {}^v v_z - d_z \end{bmatrix} + \begin{bmatrix} {}^v n \\ -{}^v u \end{bmatrix} \dot{\psi} \quad (7)$$

Image features and their dynamics

In this section, we first define visual features and then derive their dynamics in the virtual image plane, which is used in our IBVS approaches.

For the image-based control of a quadrotor, it is common to have a planar object as target.^{5,12,13,20} With this condition for the image target, image moments m_{ij} of the target with N image points are defined as follows²¹

$$m_{ij} = \sum_{k=1}^N u_k^i n_k^j \quad (8)$$

while the centered moments are given by

$$\mu_{ij} = \sum_{k=1}^N (u_k - u_g)^i (n_k - n_g)^j \quad (9)$$

where $u_g = m_{10}/m_{00}$ and $n_g = m_{01}/m_{00}$. Now we select our image features for the translational motion control of the robot as follows¹⁷

$$q_x = q_z \frac{{}^v u_g}{\lambda}, \quad q_y = q_z \frac{{}^v n_g}{\lambda}, \quad q_z = \sqrt{a^*} \quad (10)$$

where a^* is the desired value of a , which is defined as $a = \mu_{20} + \mu_{02}$. Using equation (7) and knowing ${}^v z \sqrt{a} = z^* \sqrt{a^*}$, where z^* is the desired normal distance of the camera from the target, dynamics of the features in the new image plane will be¹⁷

$$\dot{\mathbf{q}} = -sk(\dot{\psi} \mathbf{e}_3) \begin{bmatrix} q_x \\ q_y \\ q_z^D \end{bmatrix} - \frac{1}{z^*} \mathbf{v} + \frac{1}{z^*} \Delta_1 \quad (11)$$

where $\mathbf{q} = [q_x \quad q_y \quad q_z]^T$ is the vector of image features defined in equation (10) and observed in the virtual image plane and q_z^D can be an arbitrary value that is defined properly to produce image space error in section ‘‘Observer-based IBVS using image features as outputs.’’ Note that, in some applications, when the geometric model of the target is not available and only a desired image of it exists for the IBVS task, the parameter z^* will be an unknown term in equation (11). It should also be noted that the distance of O_v with respect to the virtual image plane is not necessary to be equal to λ . Therefore, λ in equations (6), (7) and (10) can be an arbitrary value. Having the same λ for both defined image planes will provide a similar demonstration in the result, and hence a suitable comparison can be made.

Observer-based IBVS using image features as outputs

In this section, we present two output feedback IBVS schemes for the 3D translational motion control of quadrotor helicopters. In the first approach, the controller does not explicitly employ angular velocity as its input and is adapted for the case in which the target is moving. Hence, the approach is developed so that it is robust with respect to (1) the unknown depth value z^* and (2) motion of the target. In the second approach, in which angular velocity data are used, an adaptive scheme is designed in order to compensate the depth uncertainty if the target is stationary. In both approaches, the objective is to move the camera, which is attached to the quadrotor, to match the observed image features with the predefined desired image features obtained from the target. The target is considered to have 3D translational motion and yaw rotation. For example, the target can be a wheeled mobile robot moving on a flat ground or a quadrotor flying with small variations in the roll and pitch angles. These kinds of target motion satisfy our assumption to have a planar image target. It is also possible to control the yaw rotation of the robot through visual information as done in Jabbari Asl et al.,¹⁴ but here we assume that the yaw rotation is controlled by IMU data in order to have a stable velocity.

Before designing the controllers, it is assumed that the camera frame, \mathcal{C} , is coincident with the quadrotor body-fixed frame, \mathcal{B} . If this condition does not hold, only a constant transformation between the two frames is needed. To design the controllers, first we need to define an error vector in the image space. In order to simplify the design procedure in the sequel, we consider the case in which our desired image features are as follows

$$\mathbf{q}^d = [q_x^d \ q_y^d \ q_z^d]^T = [0 \ 0 \ q_z^d]^T \quad (12)$$

It is common in visual servoing of quadrotor to have the observed target in the center of the image plane. This task for our selected image features, equation (10), will lead to $q_x^d = q_y^d = 0$. As done by Jabbari Asl et al.,¹⁴ it is also possible to consider another projection operator instead of equation (6) so that the desired features in the virtual image plane become equal to equation (12) for any desired features in the image plane. Now we define the image error for the translational motion control of the robot as follows

$$\delta = \mathbf{q} - [0 \ 0 \ q_z^d]^T \quad (13)$$

Using equation (11) and assigning $q_z^D = q_z - q_z^d$, the derivative of the image error vector will be

$$\dot{\delta} = -sk(\dot{\psi}\mathbf{e}_3)\delta - \frac{1}{z^*}\mathbf{v} + \frac{1}{z^*}\Delta_1 \quad (14)$$

In order to write the full translational dynamics of the image features in the virtual plane, we use the translational dynamics of the robot, equation (2), expressed in the virtual frame. Then, we have

$$\dot{\mathbf{v}} = -sk(\dot{\psi}\mathbf{e}_3)\mathbf{v} - \mathbf{f} \quad (15)$$

where \mathbf{f} is defined as follows

$$\mathbf{f} = -\mathbf{R}_{\varphi\theta}\mathbf{F}$$

In order to design a controller for the dynamics presented by equations (14) and (15), a measurement of the velocity \mathbf{v} is required. Since our objective is to design the IBVS controller without using linear velocity of the robot obtained from accelerometers, we will use the time derivative of the image features as the velocity information. This information, $\dot{\mathbf{q}}$ hence $\dot{\delta}$, can be computed by directly measuring the optic flow of each target point in the image sequence and also using the time derivatives of equations (8) and (9). There are quite a good number of researches on the methods of the robust computation of optic flow.^{22,23} However, in this article, we use a linear observer to estimate this information where the error of the estimation is considered in the stability analysis.

Now, we wish to rewrite the dynamics of the system based on available visual measurements. Therefore, by differentiating equation (14) and by substituting equation (15) in it, the dynamics of the system can be presented based on the dynamics of the visual features as follows

$$\ddot{\delta} + \mathbf{M}_1\dot{\delta} + \mathbf{M}_2\delta + \frac{1}{z^*}sk(\dot{\psi}\mathbf{e}_3)\Delta_1 + \frac{1}{z^*}\dot{\Delta}_1 = \frac{1}{z^*}\mathbf{f} \quad (16)$$

where we have

$$\mathbf{M}_1 = 2sk(\dot{\psi}\mathbf{e}_3)$$

$$\mathbf{M}_2 = sk(\ddot{\psi}\mathbf{e}_3) + sk(\dot{\psi}\mathbf{e}_3)sk(\dot{\psi}\mathbf{e}_3)$$

In many applications, the information related to the motion of the target, Δ_1 and $\dot{\Delta}_1$, is unknown, unless there is a connection between the target and the robot, where the target is equipped with appropriate measurement units. Hence, in this article, these terms are considered as unknown bounded values. As discussed in the previous section, another uncertainty in equation (16) is z^* , which is the vertical distance of the target from the robot in a desired position. Our proposed IBVS schemes are designed so as to deal with these uncertainties.

To design the controllers, we define a new set of state variables as follows

$$\xi = \delta - \hat{\delta} \quad (17)$$

$$\mathbf{s} = \dot{\delta} + \delta_1 \quad (18)$$

$$\mathbf{r} = \dot{\xi} + \xi_1 \quad (19)$$

where $\delta_1 = \eta\delta$, $\xi_1 = \eta\xi$, η is a positive constant and $\hat{\delta}$ denotes the estimate of δ . Also, the following linear

observer is used to estimate the velocity of the features²⁴

$$\begin{cases} \dot{\hat{\delta}} = \delta_o + l_d \xi \\ \dot{\delta}_o = \eta l_p \xi \end{cases} \quad (20)$$

where l_d is a positive constant. It should be noted that although the states \mathbf{s} and \mathbf{r} are not obtained by measurement, we have $\mathbf{s} - \mathbf{r} = \hat{\delta} + \eta \hat{\delta}$ from equations (17) to (19), which can be measured from visual data, and equation (20). Now, using equations (16)–(20), the dynamics of the states \mathbf{s} and \mathbf{r} can be written as

$$\begin{aligned} \dot{\mathbf{s}} = & \frac{1}{z^*} \mathbf{f} - \mathbf{M}_1 \mathbf{s} + \eta \mathbf{s} + \mathbf{M}_1 \delta_1 - \mathbf{M}_2 \frac{\delta_1}{\eta} - \eta \delta_1 \\ & - \frac{1}{z^*} sk(\dot{\psi} \mathbf{e}_3) \Delta_1 - \frac{1}{z^*} \dot{\Delta}_1 \end{aligned} \quad (21)$$

$$\begin{aligned} \dot{\mathbf{r}} = & \frac{1}{z^*} \mathbf{f} - l_d \mathbf{r} + \eta \mathbf{r} - \mathbf{M}_1 \mathbf{s} + \mathbf{M}_1 \delta_1 - \mathbf{M}_2 \frac{\delta_1}{\eta} - \eta \xi_1 \\ & - \frac{1}{z^*} sk(\dot{\psi} \mathbf{e}_3) \Delta_1 - \frac{1}{z^*} \dot{\Delta}_1 \end{aligned} \quad (22)$$

The time derivative of the yaw can be computed using equation (1) and outputs of an IMU system. Since this value is available with a high frequency, it is possible to numerically differentiate it in order to measure the acceleration of the yaw. However, in some cases, when the IMU system includes low-cost and low-weight gyroscopes, the rate information is augmented with noise and the differentiation does not provide reliable data for the control process. Hence, we will design two different image-based controllers for the translational motion of the quadrotor for the cases in which the acceleration of the yaw is available with a high accuracy or it does not include proper information for a control task.

First controller for IBVS control of the translational motion

In this section, we propose an IBVS controller for the translational motion of the robot, which uses the output feedback technique and assumes known bounds for the derivatives of the yaw angle of the robot. We also provide a controller for the yaw rotation in order to satisfy these bounds.

Now we state the following theorem:

Theorem 1. Consider the system defined by equation (16) with its input as \mathbf{f} , the states and the observer of which are defined through equations (17)–(20). Assume that $\|\mathbf{M}_1\| \leq \mu_1$, $\|\mathbf{M}_2\| \leq \mu_2$, $\|\Delta_1\| \leq D_1$, $\|\dot{\Delta}_1\| \leq D_2$ and z_{\min}^* and z_{\max}^* to be bounds on the minimum and maximum values of z^* . The following IBVS controller is proposed

$$\mathbf{f} = k_r \mathbf{r} - k_r \mathbf{s} + \mathbf{u}_1 \quad (23)$$

where \mathbf{u}_1 is defined as follows

$$\mathbf{u}_1 = \begin{cases} -D_M \frac{\hat{\mathbf{s}} + \hat{\mathbf{r}}}{\|\hat{\mathbf{s}} + \hat{\mathbf{r}}\|}, & \text{if } \|\hat{\mathbf{s}} + \hat{\mathbf{r}}\| > \varepsilon \\ -\frac{D_M}{\varepsilon} (\hat{\mathbf{s}} + \hat{\mathbf{r}}), & \text{if } \|\hat{\mathbf{s}} + \hat{\mathbf{r}}\| \leq \varepsilon \end{cases} \quad (24)$$

in which, ε is a positive constant, $D_M = \mu_1 D_1 + D_2$ and $\hat{\mathbf{s}} + \hat{\mathbf{r}} = \hat{\delta} + \eta \hat{\delta}$. Also, the controller and observer parameters k_r , η and l_d are selected in such a way that the parameters defined in the following become positive

$$\begin{aligned} A_{p1} &= \frac{k_r}{2z^*} - \mu_1 - \frac{\mu_2}{\eta} - \frac{\eta}{2} \\ B_{p1} &= \frac{k_r}{2z^*} - \mu_1 - \frac{\mu_2}{2\eta} - \frac{3\eta}{2} \\ C_{p1} &= l_d - \frac{3k_r}{2z^*} - \mu_1 - \frac{\mu_2}{2\eta} - \frac{3\eta}{2} \end{aligned} \quad (25)$$

Then the system states δ , ξ , \mathbf{s} and \mathbf{r} are UUB. Moreover, the ultimate bound can be arbitrarily made small.

Proof. Since the convergence of the states δ_1 and ξ_1 to 0 is equal to the convergence of the states δ and ξ , we use the following Lyapunov function in order to show the stability properties of the system

$$L_1 = \frac{1}{2\eta z^*} k_r \delta_1^T \delta_1 + \frac{1}{2} \mathbf{s}^T \mathbf{s} + \frac{1}{2\eta z^*} k_r \xi^T \xi + \frac{1}{2} \mathbf{r}^T \mathbf{r} \quad (26)$$

Using equations (18), (19), (21) and (22), the time derivative of equation (26) will be

$$\begin{aligned} \dot{L}_1 = & \frac{k_r}{z^*} \delta_1^T (\mathbf{s} - \delta_1) \\ & + \mathbf{s}^T \left(\frac{1}{z^*} \mathbf{f} - \mathbf{M}_1 \mathbf{s} + \eta \mathbf{s} + \mathbf{M}_1 \delta_1 - \mathbf{M}_2 \frac{\delta_1}{\eta} - \eta \delta_1 - \frac{1}{z^*} \mathbf{D} \right) \\ & + \frac{k_r}{z^*} \xi_1^T (\mathbf{r} - \xi_1) \\ & + \mathbf{r}^T \left(\frac{1}{z^*} \mathbf{f} - l_d \mathbf{r} + \eta \mathbf{r} - \mathbf{M}_1 \mathbf{s} + \mathbf{M}_1 \delta_1 - \mathbf{M}_2 \frac{\delta_1}{\eta} - \eta \xi_1 - \frac{1}{z^*} \mathbf{D} \right) \end{aligned} \quad (27)$$

where $\mathbf{D} = sk(\dot{\psi} \mathbf{e}_3) \Delta_1 + \dot{\Delta}_1$. Substituting the controller equation (23) in equation (27) and knowing that \mathbf{M}_1 is a skew-symmetric matrix, which has the property of $\mathbf{x}^T \mathbf{M}_1 \mathbf{x} = 0 \forall \mathbf{x} \in \mathbb{R}^3$, we will have

$$\begin{aligned} \dot{L}_1 = & -\frac{k_r}{z^*} \delta_1^T \delta_1^T - \left(\frac{k_r}{z^*} - \eta \right) \mathbf{s}^T \mathbf{s} - \frac{k_r}{z^*} \xi_1^T \xi_1 \\ & - \left(l_d - \eta - \frac{k_r}{z^*} \right) \mathbf{r}^T \mathbf{r} + \frac{k_r}{z^*} \delta_1^T \mathbf{s} \\ & + \mathbf{s}^T \mathbf{M}_1 \delta_1 - \mathbf{s}^T \mathbf{M}_2 \frac{\delta_1}{\eta} - \eta \mathbf{s}^T \delta_1 \\ & + \frac{k_r}{z^*} \xi_1^T \mathbf{r} - \mathbf{r}^T \mathbf{M}_1 \mathbf{s} + \mathbf{r}^T \mathbf{M}_1 \delta_1 - \mathbf{r}^T \mathbf{M}_2 \frac{\delta_1}{\eta} \\ & - \eta \mathbf{r}^T \xi_1 + \frac{1}{z^*} (\mathbf{s}^T + \mathbf{r}^T) (\mathbf{u}_1 - \mathbf{D}) \end{aligned} \quad (28)$$

Using the bounds defined for the norms of the matrices \mathbf{M}_1 and \mathbf{M}_2 , equation (28) can be bounded as follows

$$\begin{aligned} \dot{L}_1 \leq & -\frac{k_r}{z^*} \|\delta_1\|^2 - \left(\frac{k_r}{z^*} - \eta\right) \|\mathbf{s}\|^2 - \frac{k_r}{z^*} \|\xi_1\|^2 \\ & - \left(l_d - \eta - \frac{k_r}{z^*}\right) \|\mathbf{r}\|^2 + \frac{k_r}{z^*} \|\delta_1\| \|\mathbf{s}\| \\ & + \mu_1 \|\delta_1\| \|\mathbf{s}\| + \frac{\mu_2}{\eta} \|\delta_1\| \|\mathbf{s}\| + \eta \|\delta_1\| \|\mathbf{s}\| \\ & + \frac{k_r}{z^*} \|\xi_1\| \|\mathbf{r}\| + \mu_1 \|\mathbf{s}\| \|\mathbf{r}\| + \mu_1 \|\delta_1\| \|\mathbf{r}\| \\ & + \frac{\mu_2}{\eta} \|\delta_1\| \|\mathbf{r}\| + \eta \|\xi_1\| \|\mathbf{r}\| + \frac{1}{z^*} (\mathbf{s}^T + \mathbf{r}^T) (\mathbf{u}_1 - \mathbf{D}) \end{aligned} \tag{29}$$

Then, knowing the fact that $\forall \mathbf{x}_1, \mathbf{x}_2 \in \mathbb{R}^n$ and $k > 0$, $k\|\mathbf{x}_1\| \|\mathbf{x}_2\| \leq (k/2)\|\mathbf{x}_1\|^2 + (k/2)\|\mathbf{x}_2\|^2$, we can write equation (29) as follows

$$\begin{aligned} \dot{L}_1 \leq & -A_{p1} \|\delta_1\|^2 - B_{p1} \|\mathbf{s}\|^2 - \left(\frac{k_r}{2z^*} - \frac{\eta}{2}\right) \|\xi_1\|^2 \\ & - C_{p1} \|\mathbf{r}\|^2 + \frac{1}{z^*} (\mathbf{s}^T + \mathbf{r}^T) (\mathbf{u}_1 - \mathbf{D}) \end{aligned} \tag{30}$$

Now, by defining $\mathbf{x} = [\delta_1^T \quad \mathbf{s}^T \quad \xi_1^T \quad \mathbf{r}^T]^T$, equation (26) satisfies

$$h_1 \|\mathbf{x}\|^2 \leq L_1 \leq h_2 \|\mathbf{x}\|^2$$

where $h_1 = \min\{1/2, k_r/2\eta z^*\}$ and $h_2 = \max\{1/2, k_r/2\eta z^*\}$. It is known that for the Lyapunov function L_1 , if $\dot{L}_1(t) \leq 0$ for $t \geq t_0$, then the norm of \mathbf{x} is bounded by

$$\|\mathbf{x}\| \leq \sqrt{\frac{h_2}{h_1}} \|\mathbf{x}(t_0)\|$$

On the other hand, we know that $\|\mathbf{s}\| + \|\mathbf{r}\| \leq 2\|\mathbf{x}\|$ and $\|\mathbf{u}_1\| \leq D_M$, then we can write equation (30) as follows

$$\dot{L}_1 \leq -\beta_1 \|\mathbf{x}\|^2 + \beta_2 \|\mathbf{x}\| \tag{31}$$

where $\beta_1 = \min\{A_{p1}, B_{p1}, C_{p1}\}$ and $\beta_2 = 4D_M/z^*$. From equation (31), it is clear that \dot{L}_1 will be negative for $\|\mathbf{x}\| \geq \beta_2/\beta_1$ and then, provided that $\|\mathbf{x}(0)\| \leq \beta_2/\beta_1$, the norm of \mathbf{x} will be bounded as follows

$$\|\mathbf{x}\| \leq \sqrt{\frac{h_2 \beta_2}{h_1 \beta_1}} \tag{32}$$

where this bound can be arbitrarily made small by adjusting the controller and observer gains.

According to equation (25), the minimum and maximum values of z^* are required in the theorem in order to select the controller and observer gains in such a way that the parameters in equation (25) become positive.

Remark 1. If the input \mathbf{u}_1 is removed from the controller equation (23), the stability analysis is still valid and the only change is that in this case, we will have $\beta_2 = 2D_M/z^*$. However, \mathbf{u}_1 acts like a robustifying term that tries to avoid using large gains in order to deal with the uncertainty. The effect of this term is studied in section ‘‘Simulation results,’’ which shows an improvement in performance, as a smaller bound for the final values of the errors.

Remark 2. The parameters η , k_r and l_d can be used to adjust the convergence rate and the ultimate bound of the closed-loop system. Examining equation (32) and the elements of the vector \mathbf{x} shows that the larger value of η , the more the convergence rate and the less the ultimate bound of the vector of the states of the system including δ , ξ , \mathbf{s} and \mathbf{r} will be. On the other hand, the gains k_d and l_d should be selected large enough to provide a positive value for the parameters defined in equation (25). The large values of these gains increase β_1 and this in turn leads to a larger value of convergence rate and a smaller size of ultimate bound. However, it should be noted that the control parameters cannot be selected arbitrarily large in practice since existence of noise in the measurement data will produce unsatisfactory behavior.

Since the robot is underactuated, the input \mathbf{f} is unable to assign the desired dynamics directly. However, when desired \mathbf{f} is available, it is always possible to extract the trust, U_1 , and desired attitude,²⁵ namely, the roll and pitch angles, which are already assumed to be controlled with a high-gain inner-loop controller.

Now, we present a controller for the dynamics of the yaw rotation, which can help to satisfy the bounds defined in Theorem 1. Supposing small angles for the roll and the pitch, from equation (1), a good approximation for the time derivative of the yaw can be obtained as $\dot{\psi} \approx \Omega_3$. Then, one can write the dynamics of $\dot{\psi}$ as follows

$$\ddot{\psi} = \dot{\Omega}_3 + \Delta_2$$

where Δ_2 can be assumed a known bound that includes the dynamics of the neglected terms in the above approximation. In order to design a controller for the velocity of the yaw, we define the following error signal

$$e_{\dot{\psi}} = \dot{\psi} - \dot{\psi}_d \tag{33}$$

Using equation (3) and by assuming a constant desired velocity for the yaw, the time derivative of $e_{\dot{\psi}}$ will be

$$\dot{e}_{\dot{\psi}} = \ddot{\psi} = \frac{J_{xx} - J_{yy}}{J_{zz}} \Omega_1 \Omega_2 + \frac{U_4}{J_{zz}} + \Delta_2 \tag{34}$$

Now, consider the following controller

$$U_4 = (J_{yy} - J_{xx}) \Omega_1 \Omega_2 - k_{\dot{\psi}} J_{zz} e_{\dot{\psi}} \tag{35}$$

where $k_{\dot{\psi}}$ is a positive constant. By substituting equation (35) in equation (34), we will have

$$\dot{e}_{\dot{\psi}} = -k_{\dot{\psi}}J_{zz}e_{\dot{\psi}} + \Delta_2 \quad (36)$$

Then, by solving equation (36) and using equation (33), the time evolution of $\dot{\psi}$ will be

$$\dot{\psi}(t) = \dot{\psi}_d + e_{\dot{\psi}}(0)e^{-k_{\dot{\psi}}J_{zz}t} + \frac{\Delta_2}{k_{\dot{\psi}}J_{zz}}(1 - e^{-k_{\dot{\psi}}J_{zz}t})$$

which can be bounded as follows

$$\dot{\psi}(t) \leq \dot{\psi}_d + e_{\max}$$

where $e_{\max} = |e_{\dot{\psi}}(0)| + |\Delta_2|/(k_{\dot{\psi}}J_{zz})$. Then, the controller equation (35) for the velocity of the yaw sets a bound for the maximum value of $\dot{\psi}$, which can be used to compute μ_1 .

On the other hand, since $\ddot{\psi} = \dot{e}_{\dot{\psi}}$, from equation (36), we will have

$$\ddot{\psi} = -k_{\dot{\psi}}J_{zz}e_{\dot{\psi}} + \Delta_2$$

which can be bounded as

$$\ddot{\psi} \leq k_{\dot{\psi}}J_{zz}e_{\max} + \Delta_2$$

This indicates that the controller equation (35) also provides a maximum value for $\ddot{\psi}$, which can satisfy the required bound μ_2 . Note that the controller gain $k_{\dot{\psi}}$ can be used to adjust maximum values of $\dot{\psi}$ and $\ddot{\psi}$.

Remark 3. Since the controller equation (23) does not employ angular velocities to compute the force input \mathbf{f} for controlling the translational motion, it has advantage over the approach developed in Mahony et al.¹⁵ where translational optic flow is used as the velocity information. The translational optic flow can be computed from optic flow of the image after correcting the angular optic flow, which requires angular velocity information. Therefore, in the case that the outputs of the rate gyroscopes are corrupted by noise, the output signals generated by the controller will contain a significant amount of noise, which may destabilize the system. It should be noted that in this case, the angles are still reliable since they are filtered outputs of the gyroscopes through the integration.

Second controller for IBVS control of the translational motion

Now, we present the second IBVS controller that uses the velocity and the acceleration of the yaw rotation in controlling the translational motion of the quadrotor. Using these information, it is possible to release the assumed bound on the yaw acceleration and also the control gains will require less restrictive conditions. Here, we consider the case that the target is stationary; hence, we will have $\Delta_1 = \dot{\Delta}_1 = 0$. Now, the following theorem is stated.

Theorem 2. Consider the system defined by equation (16) with the states δ , ξ , \mathbf{s} and \mathbf{r} and its input as \mathbf{f} . Under the assumption that $\|\mathbf{M}_1\| \leq \mu_1$, and z_{\min}^* and z_{\max}^* are bounds on the minimum and maximum values of z^* , the following IBVS controller is proposed

$$\mathbf{f} = k_r\mathbf{r} - k_r\mathbf{s} - \eta\hat{z}^*\mathbf{M}_1\delta + \hat{z}^*\mathbf{M}_2\delta \quad (37)$$

in which the control and observer gains k_r , η and l_d are selected so that satisfy the following conditions

$$\begin{aligned} k_r &> z_{\max}^*(3\eta + \mu_1) \\ l_d &> \frac{3k_r}{2z_{\min}^*} + \frac{3\eta}{2} + \frac{\mu_1}{2} \end{aligned} \quad (38)$$

and also \hat{z}^* is an estimated value of z^* , which is updated with the following adaptation law

$$\dot{\hat{z}}^* = \gamma(\mathbf{s}^T + \mathbf{r}^T) \left(\mathbf{M}_1\delta_1 - \mathbf{M}_2\frac{\delta_1}{\eta} \right) \quad (39)$$

where γ is a positive constant. Then, the system states are UUB and converge asymptotically to 0.

Proof. We consider the following Lyapunov function

$$\begin{aligned} L_2 &= \frac{k_r}{2\eta z^*} \delta_1^T \delta_1 + \frac{1}{2} \mathbf{s}^T \mathbf{s} + \frac{k_r}{2\eta z^*} \xi_1^T \xi_1 \\ &+ \frac{1}{2} \mathbf{r}^T \mathbf{r} + \frac{1}{2\gamma z^*} \tilde{z}^* \tilde{z}^* \end{aligned} \quad (40)$$

where $\tilde{z}^* = z^* - \hat{z}^*$. The time derivative of equation (40) will be

$$\begin{aligned} \dot{L}_2 &= \frac{k_r}{z^*} \delta_1^T (\mathbf{s} - \delta_1) \\ &+ \mathbf{s}^T \left(\frac{1}{z^*} \mathbf{f} - \mathbf{M}_1 \mathbf{s} + \eta \mathbf{s} + \mathbf{M}_1 \delta_1 - \mathbf{M}_2 \frac{\delta_1}{\eta} - \eta \delta_1 \right) \\ &+ \frac{k_r}{z^*} \xi_1^T (\mathbf{r} - \xi_1) \\ &+ \mathbf{r}^T \left(\frac{1}{z^*} \mathbf{f} - l_d \mathbf{r} + \eta \mathbf{r} - \mathbf{M}_1 \mathbf{s} + \mathbf{M}_1 \delta_1 - \mathbf{M}_2 \frac{\delta_1}{\eta} - \eta \xi_1 \right) \\ &- \frac{\tilde{z}^*}{\gamma z^*} \dot{\tilde{z}}^* \end{aligned} \quad (41)$$

After substituting equation (37) in equation (41), it can be bounded as follows

$$\begin{aligned} \dot{L}_2 &\leq -\frac{k_r}{z^*} \|\delta_1\|^2 - \left(\frac{k_r}{z^*} - \eta \right) \|\mathbf{s}\|^2 - \frac{k_r}{z^*} \|\xi_1\|^2 \\ &- \left(l_d - \eta - \frac{k_r}{z^*} \right) \|\mathbf{r}\|^2 + \frac{k_r}{z^*} \|\delta_1\| \|\mathbf{s}\| + \eta \|\delta_1\| \|\mathbf{s}\| \\ &+ \frac{k_r}{z^*} \|\xi_1\| \|\mathbf{r}\| + \mu_1 \|\mathbf{s}\| \|\mathbf{r}\| + \eta \|\xi_1\| \|\mathbf{r}\| \\ &+ \frac{\tilde{z}^*}{z^*} \left[(\mathbf{s}^T + \mathbf{r}^T) \left(\mathbf{M}_1 \delta_1 - \mathbf{M}_2 \frac{\delta_1}{\eta} \right) - \frac{1}{\gamma} \dot{\tilde{z}}^* \right] \end{aligned} \quad (42)$$

Substituting equation (39) in equation (42), considering the specified conditions for the control gains in

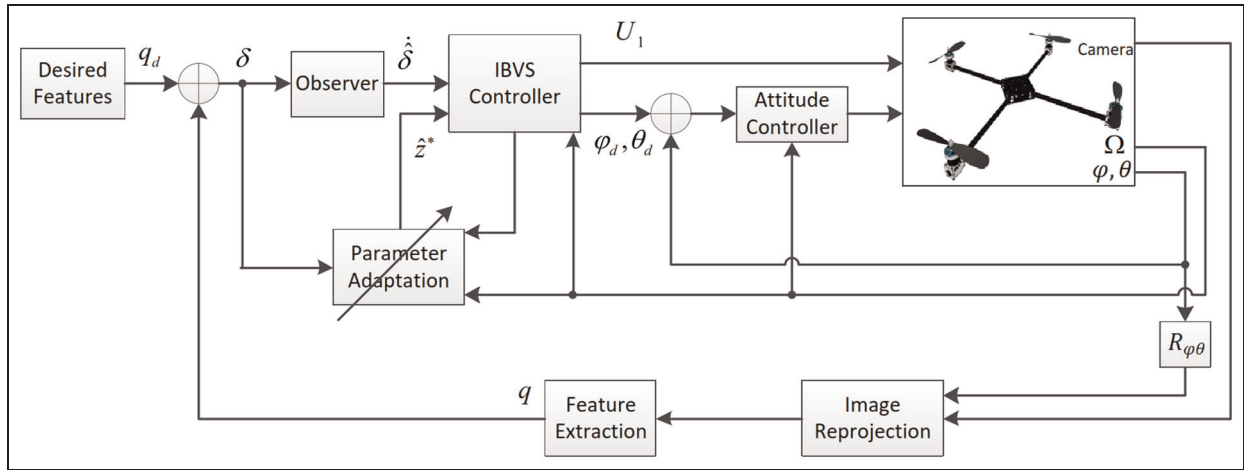


Figure 3. Block diagram of the second IBVS scheme for the translational motion control. IBVS: image-based visual servoing.

equation (38) and using the same property, which is implemented to obtain equation (30), we can reach

$$\dot{L}_2 \leq -A_{p2} \|\delta_1\|^2 - B_{p2} \|\mathbf{s}\|^2 - A_{p2} \|\xi_1\|^2 - C_{p2} \|\mathbf{r}\|^2$$

where

$$A_{p2} = \frac{k_r}{2z^*} - \frac{\eta}{2}$$

$$B_{p2} = \frac{k_r}{2z^*} - \frac{\mu_1}{2} - \frac{3\eta}{2}$$

$$C_{p2} = l_d - \frac{3k_r}{2z^*} - \frac{\mu_1}{2} - \frac{3\eta}{2}$$

Then, we obtain the following inequality

$$\dot{L}_2 \leq -\beta_3 \|\mathbf{x}\|^2 \leq 0 \tag{43}$$

where $\beta_3 = \min\{A_{p2}, B_{p2}, C_{p2}\}$. Equation (43) implies that δ , ξ , \mathbf{s} , \mathbf{r} and \tilde{z}^* are bounded and then we have

$$\lim_{t \rightarrow \infty} \beta_3 \int_{t_0}^t \mathbf{x}^T \mathbf{x} dt \leq L_2(t_0) - L_2(\infty) < \infty$$

From equations (18), (19), (21) and (22), δ , ξ , $\dot{\mathbf{s}}$ and $\dot{\mathbf{r}}$ are also bounded. Therefore, \mathbf{x} is uniformly continuous, which, by applying Barbalat's lemma, indicates that δ , ξ , \mathbf{s} and \mathbf{r} converge to 0 asymptotically.

The adaptation law (equation (39)) contains δ , which is assumed to be unmeasurable. Integrating equation (39), the following equivalent version of equation (39) can be obtained, which does not depend on δ ²⁶

$$\begin{aligned} \tilde{z}^* &= \tilde{z}^*(0) + \gamma \int_0^t (\mathbf{s}^T + \mathbf{r}^T) \left(\mathbf{M}_1 \delta_1 - \mathbf{M}_2 \frac{\delta_1}{\eta} \right) dt \\ &= \tilde{z}^*(0) + 2\gamma \int_{\delta(0)}^{\delta(t)} \left(\mathbf{M}_1 \delta_1 - \mathbf{M}_2 \frac{\delta_1}{\eta} \right)^T d\delta \\ &\quad + \gamma \int_0^t \left(\delta_1^T + \xi_1^T - \dot{\delta}^T \right) \left(\mathbf{M}_1 \delta_1 - \mathbf{M}_2 \frac{\delta_1}{\eta} \right) dt \end{aligned}$$

The same discussion presented in Remark 2 is also valid for this approach as the tuning rules for the control parameters in order to provide a satisfactory convergence rate for the system. Block diagram of the proposed IBVS scheme is shown in Figure 3.

Remark 4. During an IBVS task, a persistent excitation condition may not be satisfied for the adaptation law (equation (39)), and therefore, the convergence of the parameter \tilde{z}^* to its true value may not be guaranteed. However, the control scheme does not require the convergence of the estimated parameter to the true value.

Simulation results

In this section, we present MATLAB simulations to evaluate the performance of the proposed observer-based visual servo controllers. In the simulations, the camera frame rate is set at 50 Hz and sampling time for the rest of the system is 10 ms. The robot is assumed to start in a hover position with the desired target in the camera's field of view. Visual information includes coordinates of four points corresponding to four vertices of a rectangle, which are used to calculate the image features defined in equation (10). Vertices of the rectangle with respect to the inertial frame are located at (0.25, 0.2, 0) m, (0.25, -0.2, 0) m, (-0.25, 0.2, 0) m and (-0.25, -0.2, 0) m. These points are projected through perspective projection on a digital image plane with focal length divided by pixel size (identical in both horizontal and vertical directions) equal to 213 and the principal point located at (80, 60).

The dynamic parameters of the robot are selected as $m = 2$ kg, $g = 9.81$ ms⁻² and $J = \text{diag}(0.0081, 0.0081, 0.0142)$ kg m² rad⁻². Also, z_{\min}^* and z_{\max}^* are assumed to be 1 and 10 m, respectively. The inverse dynamics of the quadrotor²⁷ are used to compute the desired attitude of the robot in order to provide the force inputs for the translational motion designed in equations (23) and (37). High-gain proportional-derivative controllers

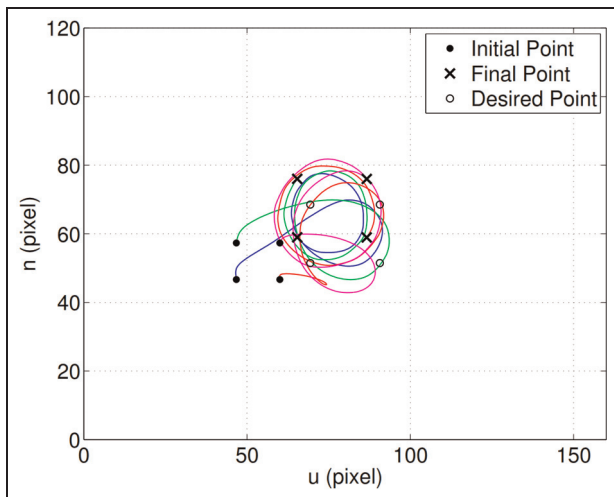


Figure 4. Simulation I: target point trajectories in the virtual image plane.

are implemented to control the desired roll and pitch angles of the robot.

Results of the first method

The first simulation demonstrates the performance of the controller given by equation (23). In this simulation, the robot's initial position is at $(0, -0.3, -8)$ m with respect to the inertial frame and the desired image features are obtained at $(0, 0, -5)$ m. The observed target is assumed to move on flat ground, following a circle of radius 1 m with a velocity of $\pi/15$ rad s⁻¹. In order to simulate the low quality of the rate gyroscopes, white noise with covariance of 10^{-4} is added to the angular velocity information. The controller and observer gains are set as $k_r = 8$, $\eta = 0.2$ and $l_d = 20$. In equation (24), D_M and ε are selected to be 3 and 0.1, respectively. The desired yaw velocity is also set as 0, which is controlled by equation (35) with $k_\psi = 3J_{zz}^{-1}$. In order to simulate the effect of uncertainties in the inertia matrix, J_{xx} and J_{yy} in equation (35) are set as 0.0091 and 0.0071 kg m²/rad², respectively.

Figure 4 shows the trajectories of the image points in the virtual image plane. The norms of the error signals are illustrated in Figure 5. Trajectories of the translational motion of the robot in Cartesian coordinates and in a 3D illustration are shown in Figures 6 and 7, respectively. Also, Figure 8 shows the time evolution of the derivatives of the yaw. The results of this simulation demonstrate satisfactory tracking of the target and the error signals, and also the system states are bounded in the tracking mission and converge to the small compact sets.

In order to show the effect of the input term \mathbf{u}_1 in the performance of the system, the simulation is tested again, while this term has been removed from equation (23). For this simulation, the trajectories of the image points are demonstrated in Figure 9. Comparing

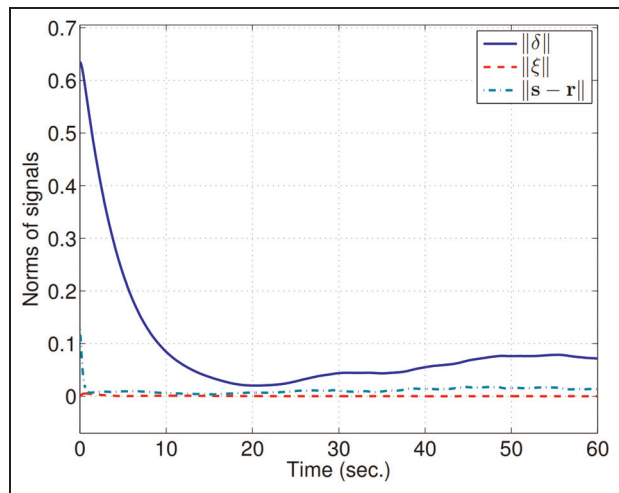


Figure 5. Simulation I: time evolution of the norms of the error vectors.

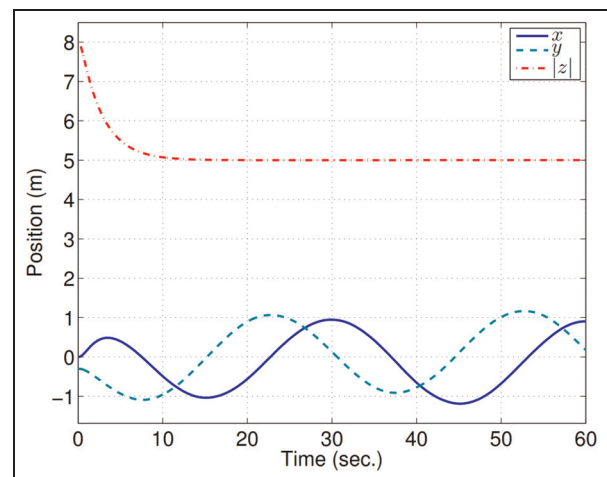


Figure 6. Simulation I: time evolution of the quadrotor Cartesian coordinates.

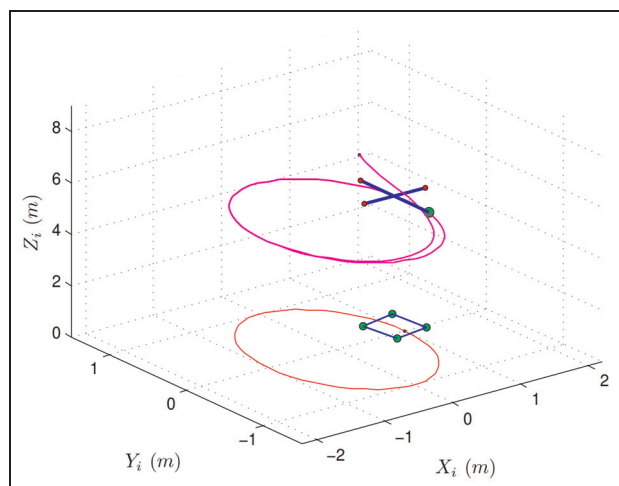


Figure 7. Simulation I: trajectory of the motion of the robot and the target in a 3D environment.

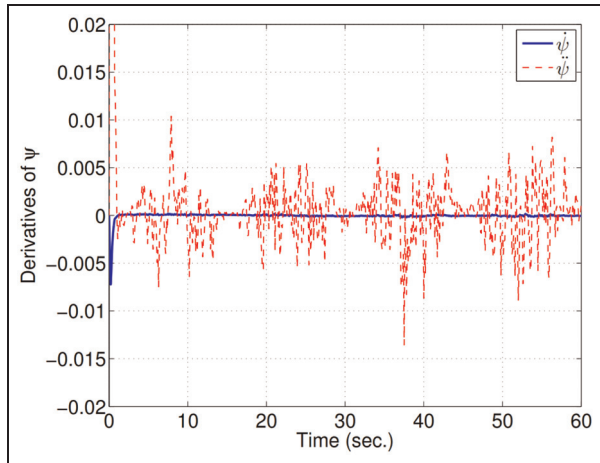


Figure 8. Simulation 1: time evolution of the derivatives of the yaw.

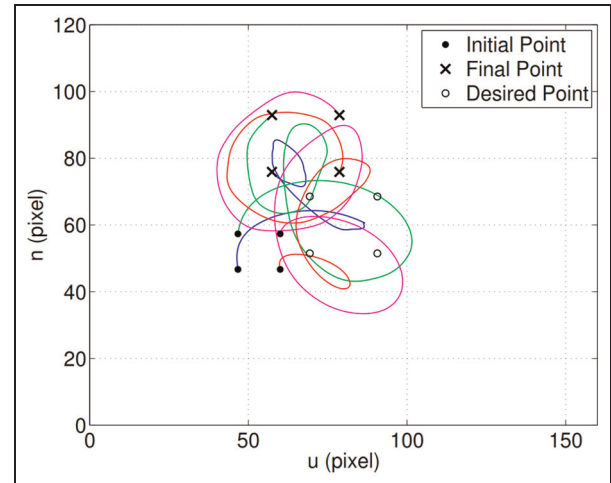


Figure 9. Simulation 1: target point trajectories in the virtual image plane when the input term u_1 has been removed from equation (23).

Figures 4 and 9 reveals the improvement achieved when using u_1 .

Results of the second method

In the second simulation, we evaluate the performance of the second controller given by equation (37). The robot initial position is considered to be at $(-0.4, -0.1, -7)$ m while the desired features are obtained at $(0, 0, -5)$ m where the target is assumed to be stationary. The controller and observer gains k_r, η and l_d are selected to be just like the previous simulation and the adaptation gain γ is set as 2. Also, the initial value for the update law equation (39) is set as $\hat{z}^*(0) = 10$ m. In this simulation, the yaw rotation of the robot is controlled using visual information through the method presented in Jabbari Asl et al.¹⁴

Figure 10 demonstrates the trajectories of the image points in the virtual image plane. Figure 11 shows the norms of the error vectors for the translational motion. Trajectories of the translational motion of the robot in Cartesian coordinates are presented in Figure 12. Also, the time evolution of \hat{z}^* is shown in Figure 13. As expected, satisfactory trajectories have been achieved in both Cartesian coordinates and the virtual image plane and also the system errors converge to 0.

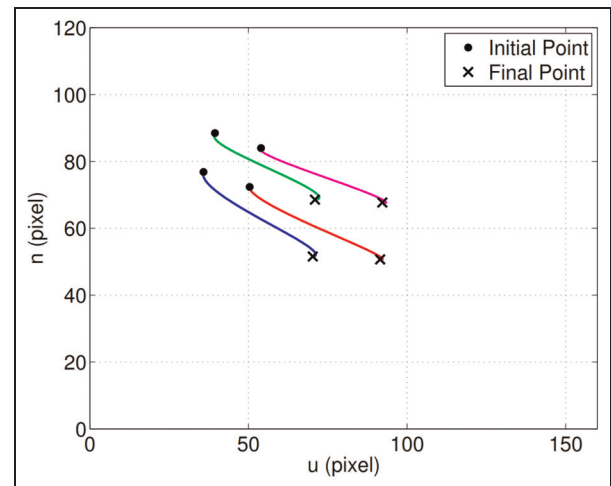


Figure 10. Simulation 2: target point trajectories in the virtual image plane.

A comparative study

In order to demonstrate the effectiveness of the proposed IBVS controllers with respect to previous methods, the results obtained from our first scheme are here compared with the results of an approach where the linear velocity information is assumed to be available through an IMU system. Since the main contribution of the errors in the linear velocities is the bias in the IMU readings,²⁸ a ramp function with the slope of 0.01 m s^{-1} (as a result of a constant bias in the accelerometers' data) is added to the linear velocity information. On the other hand, we have added some terms in

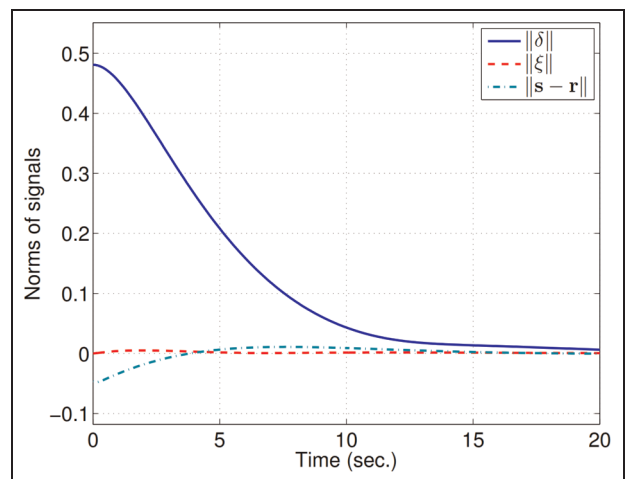


Figure 11. Simulation 2: time evolution of the norms of the error vectors.

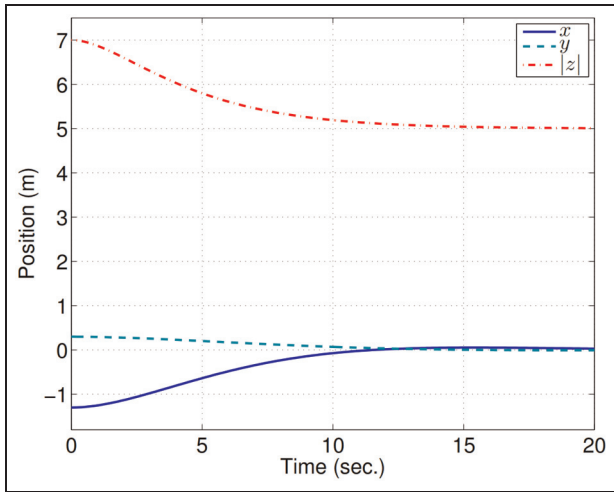


Figure 12. Simulation 2: time evolution of the quadrotor Cartesian coordinates.

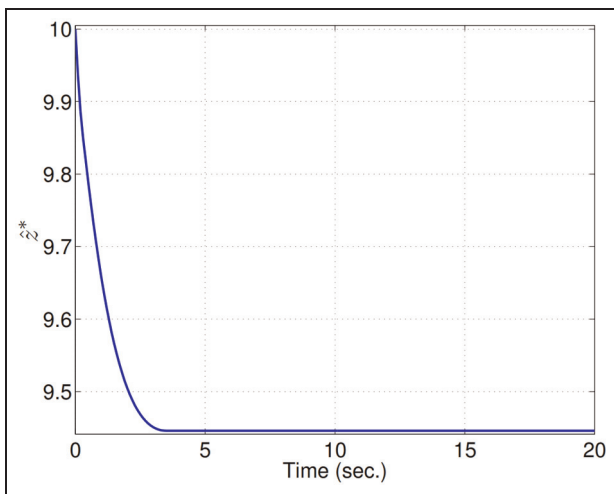


Figure 13. Simulation 2: time evolution of \hat{z}^* .

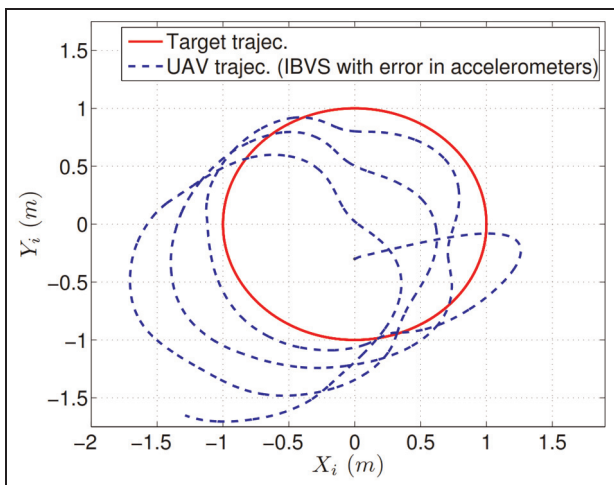


Figure 14. Simulation 3: $X_i Y_i$ plane trajectories of the target and the UAV after three rounds for a classic IBVS approach with bias error in accelerometers. UAV: unmanned aerial vehicle; IBVS: image-based visual servoing.

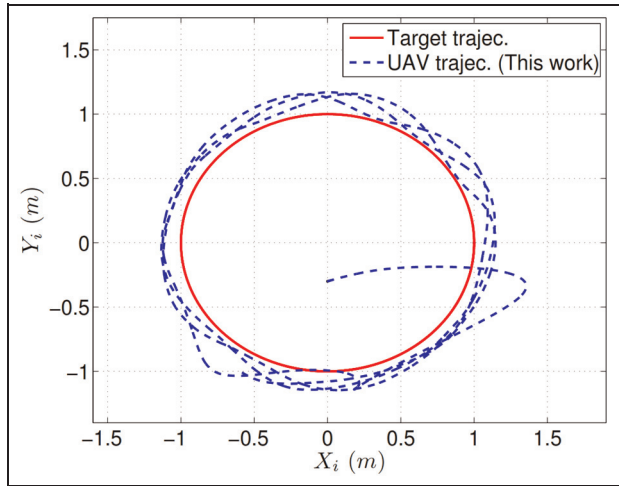


Figure 15. Simulation 3: $X_i Y_i$ plane trajectories of the target and the UAV after three rounds for the approach presented in this work.

UAV: unmanned aerial vehicle.

the simulation in order to provide more realistic conditions for our tests. These terms include a noise with covariance of 0.5 in the visual data, a time delay of 0.03 s in transmitting the visual data and also include unstructured forces and moments in the dynamics of the system, which are modeled by sinusoidal signals with different phases for each channel and amplitudes equal to 0.1 N and 0.02 N m, respectively.

For our comparative study, the classic IBVS approach, presented in Ceren and Altug,²⁹ is used to control the 3D translational motion and the yaw rotation of the quadrotor to track a target following a trajectory the same as the first simulation. The control gain for this approach is selected to provide the best performance after several simulations. In simulating our approach, the yaw rotation is controlled by the method presented in Jabbari Asl et al.,¹⁴ and the control gains are selected to be the same as the first simulation. The trajectories of the target and the robot in the $X_i Y_i$ plane for the classic approach and our proposed approach are illustrated in Figures 14 and 15, respectively. The results demonstrate that a small amount of bias in the accelerometers' data degrades the performance of the classic approach while our approach performs well in spite of considerable amount of noise and disturbance in the system.

Conclusion

In this article, two observer-based IBVS controller schemes have been developed for the translational motion of the quadrotor helicopter. Since the common IMU systems used in robotics applications do not provide appropriate quality of linear velocity, the main objective was to use the velocity of image features as the linear velocity cue. This quantity is estimated from visual features through a linear observer. The image

features are selected from perspective image moments, which are reprojected on an oriented image plane where this reprojection compensates the underactuated structure of the UAV. To design the controllers, dynamic model of the system is expressed in terms of the velocity of the image features, which make it possible to design dynamic IBVS controllers for this vehicle without using linear velocity information obtained from accelerometers. The proposed controllers are robust with respect to the uncertainties in the dynamics of the system related to depth information of the image and also motion of the target when it is moving. Stability analysis shows that the states of the system remain UUB and the errors converge to a small compact set during a tracking mission and also converge to 0 when the target is stationary. Simulation results show a satisfactory response of the presented visual servo approaches in both image space and Cartesian space of the robot even in the presence of considerable amount of noise and disturbance in the system.

In the design procedure, only the translational dynamics of the vehicle is considered and it is assumed that the rotational dynamics are controlled by high-gain controllers. However, further analysis such as time-scale separation method can also be applied in order to prove the stability of the whole system.

Our future work is devoted to design an output feedback IBVS controller by applying passivity properties of the image dynamics and using translational optic flow information of the image features. We also intend to verify the effectiveness of the proposed control algorithms in practice on a real quadrotor.

Declaration of conflicting interests

The authors declare that there is no conflict of interest.

Funding

This research received no specific grant from any funding agency in the public, commercial or not-for-profit sectors.

References

- Shakernia O, Ma Y, Koo T, et al. Landing an unmanned air vehicle: vision based motion estimation and nonlinear control. *Asian J Control* 1999; 1: 128–145.
- Mondragon I, Campoy P, Martinez C, et al. 3D pose estimation based on planar object tracking for UAVs control. In: *Proceedings of the 2010 IEEE international conference on robotics and automation*, Anchorage, AK, 3–7 May 2010, pp.35–41. New York: IEEE.
- Artieda J, Sebastian J, Campoy P, et al. Visual 3D SLAM from UAVs. *J Intell Robot Syst* 2009; 55: 299–321.
- Lee D, Ryan T and Kim HJ. Autonomous landing of a VTOL UAV on a moving platform using image-based visual servoing. In: *Proceedings of the 2012 IEEE international conference on robotics and automation*, Saint Paul, MN, 14–18 May 2012, pp.971–976. New York: IEEE.
- Hamel T and Mahony R. Visual servoing of an underactuated dynamic rigid-body system: an image-based approach. *IEEE T Robot Autom* 2002; 18: 187–198.
- Saunders J, Beard R and Byrne J. Vision-based reactive multiple obstacle avoidance for micro air vehicles. In: *Proceedings of the 2009 American control conference*, St. Louis, MO, 10–12 June 2009, pp.5253–5258. New York: IEEE.
- Altug E, Ostrowski JP and Mahony R. Control of a quadrotor helicopter using visual feedback. In: *Proceedings of the 2002 IEEE international conference on robotics and automation*, vol. 1, 11–15 May 2002, Washington, DC, USA, pp.72–77. New York: IEEE.
- Altug E, Ostrowski JP and Taylor CJ. Control of a quadrotor helicopter using dual camera visual feedback. *Int J Robot Res* 2005; 24: 329–341.
- Garca Carrillo L, Rondon E, Sanchez A, et al. Stabilization and trajectory tracking of a quad-rotor using vision. *J Intell Robot Syst* 2011; 61: 103–118.
- Janabi-Shari F and Marey M. A Kalman-filter-based method for pose estimation in visual servoing. *IEEE T Robot* 2010; 26: 939–947.
- Hamel T and Mahony R. Image based visual servo control for a class of aerial robotic systems. *Automatica* 2007; 43: 1975–1983.
- Guenard N, Hamel T and Mahony R. A practical visual servo control for an unmanned aerial vehicle. *IEEE T Robot* 2008; 24: 331–340.
- Bourquardez O, Mahony R, Guenard N, et al. Image-based visual servo control of the translation kinematics of a quadrotor aerial vehicle. *IEEE T Robot* 2009; 25: 743–749.
- Jabbari Asl H, Oriolo G and Bolandi H. Dynamic IBVS control of an underactuated UAV. In: *Proceedings of the 2012 IEEE international conference on robotics and biomimetics*, Guangzhou, China, 11–14 December 2012, pp.1158–1163. New York: IEEE.
- Mahony R, Corke P and Hamel T. Dynamic image-based visual servo control using centroid and optic flow features. *J Dyn Syst: T ASME* 2008; 130: 011005 (12 pp.).
- Le Bras F, Hamel T, Mahony R, et al. Output feedback observation and control for visual servoing of VTOL UAVs. *Int J Robust Nonlin* 2011; 21: 1008–1030.
- Jabbari Asl H, Oriolo G and Bolandi H. An adaptive scheme for image-based visual servoing of an underactuated UAV. *Int J Robot Autom* 2014; 29: 92–104.
- Tayebi A and McGilvray S. Attitude stabilization of a VTOL quadrotor aircraft. *IEEE T Contr Syst T* 2006; 14: 562–571.
- Bertrand S, Hamel T and Piet-Lahanier H. Stability analysis of an UAV controller using singular perturbation theory. In: *Proceedings of the 17th IFAC world congress*, Seoul, South Korea, 6–11 July 2008, pp.5706–5711. New York: IFAC.
- Ozawa R and Chaumette F. Dynamic visual servoing with image moments for a quadrotor using a virtual spring approach. In: *Proceedings of the 2011 IEEE international conference on robotics and automation*, Shanghai, China, 9–13 May 2011, pp.5670–5676. New York: IEEE.
- Tahri O and Chaumette F. Point-based and region-based image moments for visual servoing of planar objects. *IEEE T Robot* 2005; 21: 1116–1127.
- Srinivasan M and Zhang S. Visual motor computations in insects. *Annu Rev Neurosci* 2004; 27: 679–696.

23. Zufferey J and Floreano D. Fly-inspired visual steering of an ultralight indoor aircraft. *IEEE T Robot* 2006; 22: 137–146.
24. Berghuis H and Nijmeijer H. Robust control of robots via linear estimated state feedback. *IEEE T Automat Contr* 1994; 39: 2159–2162.
25. Abdessameud A and Tayebi A. Global trajectory tracking control of VTOL-UAVs without linear velocity measurements. *Automatica* 2010; 46(6): 1053–1059.
26. Erlic M and Lu W. A reduced-order adaptive velocity observer for manipulator control. *IEEE T Robot Automat* 1995; 11: 293–303.
27. Das A, Lewis F and Subbarao K. Backstepping approach for controlling a quadrotor using Lagrange form dynamics. *J Intell Robot Syst* 2009; 56: 127–151.
28. Bryson M and Sukkarieh S. Vehicle model aided inertial navigation for a UAV using low-cost sensors. In: *Proceedings of the 2004 Australasian conference on robotics and automation*, Canberra, ACT, Australia, 6–8 December 2004, vol. 1, pp.72–77.
29. Ceren Z and Altug E. Vision-based servo control of a quadrotor air vehicle. In: *Proceedings of the 2009 computational intelligence in robotics and automation*, Daejeon, South Korea, 15–18 December 2009, pp.84–89. New York: IEEE.

Appendix I

Notation

\mathcal{B}	body-fixed frame
\mathcal{C}	camera fixed frame
\mathbf{f}	input force of the rigid body in \mathcal{V} frame

\mathbf{F}	input force of the rigid body in \mathcal{B} frame
\mathcal{I}	inertial frame
l_d	observer gain
L_1, L_2	Lyapunov functions
m	mass of quadrotor
m_{ij}	image moments
${}^{\mathcal{V}}\mathbf{p}$	coordinates of point P in \mathcal{V} frame
${}^{\mathcal{I}}\mathbf{p}$	coordinates of point P in \mathcal{I} frame
q_x, q_y, q_z	image features
\mathbf{R}	rotation matrix
u, n	coordinates of a point in image plane
${}^{\mathcal{V}}u, {}^{\mathcal{V}}n$	coordinates of a point in virtual image plane
U_1	thrust input
\mathbf{v}	linear velocity of rigid body in \mathcal{V} frame
\mathbf{V}	linear velocity of rigid body in \mathcal{B} frame
\mathcal{V}	virtual frame
z^*	desired normal distance of the camera from the target
γ	adaptation gain
Δ_1	velocity of a moving point in the virtual frame
δ	image space error
η, k_r	control gains
λ	focal length of camera
μ_{ij}	centered image moments
Ω	angular velocity of the rigid body in \mathcal{B} frame